

High- and very high-cycle plain fatigue resistance of shot peened high-strength aluminium alloys: the role of surface morphology

M. Benedetti^{1*}, V. Fontanari¹, M. Bandini², E. Savio³

¹Department of Industrial Engineering, University of Trento, via Sommarive 9, 38123 Trento, Italy

²Peen Service s.r.l., via Pollastri 7, 40138 Bologna, Italy

³Department of Industrial Engineering, University of Padova, via Venezia 1, 35131 Padova, Italy

* Contacting Author:

Matteo Benedetti

Tel. +390461282457

Fax +390461281977

E-mail: matteo.benedetti@unitn.it

Abstract

The present paper is aimed at investigating the effect of shot peening on the high and very-high cycle plain fatigue resistance of the Al-7075-T651 alloy. Pulsating bending fatigue tests ($R = 0.05$) were carried out on smooth samples exploring fatigue lives comprised between 10^5 and 10^8 cycles. Three peening treatments were considered to explore different initial residual stress profiles and surface microstructural conditions. An extensive analysis of the residual stress field was carried out by measuring with the X-ray diffraction (XRD) technique the residual stress profile before and at the end of the fatigue tests. Fatigue crack initiation sites were investigated through scanning electron microscopy (SEM) fractography. The surface morphology modifications induced by shot peening were evaluated using an optical profilometer. The influence of surface finishing on the fatigue resistance was quantified by eliminating the surface roughness in some peened specimens through a tribofinishing treatment. The capability of shot peening to hinder the initiation and to retard the subsequent propagation of surface cracks is discussed on the basis of a model combining a multiaxial fatigue criterion and a fracture mechanics approach.

Keywords: Shot peening; very high-cycle fatigue; Al-7075-T651; residual stresses; tribofinishing

Nomenclature

Symbols

a	Surface crack depth
c	Surface crack half-width
d	Material strongest microstructural barrier
D_p	Mean spacing of adjacent roughness peaks
D_n	Notch depth
k	Factor expressing exponential crack size dependence of ΔK_{th}
K	Stress intensity factor
K_r	Residual stress intensity factor
K_t	Notch stress concentration factor
LC	Long crack
m	Weight function
MSC	Microstructurally small crack
N_f	Number of cycles to failure
p	Hydrostatic pressure
PSC	Physically small crack
R	Nominal load ratio
R_t	Maximum peak to valley height
s	Slope of the Wöhler curve
t	Specimen thickness
$T\sigma$	Stress-based scatter index (related to the 10–90% probability of survival curves)
x	Cartesian coordinate along the crack depth with origin on the sample surface
Y	Shape factor for crack stress intensity factor
α_c, β_c	Material parameters of the Crossland fatigue criterion
Δ	Range over a fatigue cycle
ΔK_{dR}	Smallest physically small crack threshold
ΔK_{th}	Crack size dependent physically small crack threshold
ΔK_{thR}	Long crack threshold stress intensity factor range

$\Delta\sigma_{eR}$	Plain fatigue strength range at high number of cycles to failure
κ	Driving force for fatigue crack propagation
σ	Normal stress
σ^{RS}	Surface residual stress
σ_0	y-intercept of the Wohler curve
σ_{VM}	Von Mises equivalent stress

Subscripts

a	Amplitude over a fatigue cycle
$appl$	Applied due to external loading
eff	Effective
max	Maximum over a fatigue cycle
min	Minimum over a fatigue cycle
P	Probability of failure
tot	Total

1. Introduction

Fatigue life of metal components is spent to nucleate and propagate a dominant crack until the final failure. Usually, crack initiation involves the formation of a defect whose size is comparable with a material's characteristic slip length [1, 2]. At this stage, the crack is referred to as microstructurally-small. The subsequent stage involves the growth of the crack that is, at first, physically-small, and then, long [3]. Therefore, the fatigue strength of a mechanical component can be improved if at least one of these two stages is prolonged. Resistance to crack initiation can be essentially improved through grain refinement (that controls the material's characteristic slip length) [4], work-, precipitation-, and solution-hardening (to withstand the formation of persistent slip bands) [5], surface polishing (to alleviate the stress concentration effect exerted by surface roughness) [6], mean stress effect [7]. Conversely, the crack propagation is impeded by extrinsic mechanisms such as crack closure, crack bridging, crack deflection and crack front geometry [8,9].

Shot peening is a surface treatment that is commonly used to take advantage of some of these effects to improve the fatigue resistance of metallic materials. This process consists of bombarding the component with small spherical shots of a hard material at a relatively high velocity. Clearly, the multiple indentation of the ductile

target surface increases its surface roughness, but, if shot peening is correctly performed, the detrimental effect exerted on the crack nucleation resistance is outweighed by several beneficial modifications of the surface layers. Specifically, (i) the introduction of an in-plane compressive residual stress field hinders crack nucleation owing to mean stress effect [10] and retards the propagation of Physically-Small Cracks (PSC) [10-13] restoring, at least partially, crack closure that in PSC is not fully developed as in Long Cracks (LC) [14]. Obviously, the beneficial effects exerted by compressive residual stresses strongly depend upon their stability throughout the fatigue life [15]. In this regard, re-orientation and change in the magnitude of the residual strain field was found as a consequence of cyclic loading [16]. (ii) Work-hardening and the resulting increase in the near-surface dislocation density retard crack nucleation but often accelerate crack propagation due to material embrittlement [17,18]. (iii) Depending on the treatment intensity, shot peening causes more or less evident microstructural changes; among them, near-surface grain refinement (thus reducing the maximum dislocation slip length and therefore incrementing the resistance to crack initiation) [19], elongated and flattened grains near the peened surface [20], changes in the orientation of precipitates [21], modification of the near-surface crystallographic texture [22], stress-induced martensitic transform [23]. The grain refinement effect has been explored in recent works in order to create nanostructured surfaces through very intense peening treatments [24].

Clearly, shot peening is a surface treatment able to modify the mechanical and microstructural characteristics of the near-surface material layers. Therefore, in many cases, especially in the high-cycle ($10^5 < N_f < 10^7$) and very-high-cycle ($N_f > 10^7$) fatigue regime, shot peening suppresses surface crack initiation and pushes the crack source beneath the hardened surface layers [17,21,25-30]. Preferential sites for subsurface crack initiation were found to be non-metallic inclusions [25-28,30], pores [31], the region where superimposed residual and external stresses are maximum [17] or exceed the local material's yield strength [21].

The need for fatigue strength improvement is particularly felt in Al-alloys, because their elevated specific static strength does not reflect equally high fatigue properties [4,32,33]. Their scarce fatigue resistance is imputed to (i) weak microstructural barriers to the propagation of Microstructurally-Small Cracks (MSC) [34] and (ii) a high notch sensitivity [33], making them very susceptible to the stress concentration exerted by surface roughness. Therefore, in Al-alloys the majority of fatigue cracks initiate on the surface. For these reasons, the surface modification through shot peening is an attractive method of improving fatigue performance of Al-alloys. Over the last decades, considerable research effort has been devoted to identifying the most effective peening treatments for high-strength Al-alloys [17,21,29,35-39]. It is commonly accepted that gentle treatments employing small ceramic beads induce the highest fatigue life enhancement, mainly for the following reasons: (i)

the compressive residual stress peak is located close to the surface where the cracks are likely to nucleate, (ii) strain hardening is concentrated near the surface and helps maintaining stable the residual stress field in the region of crack initiation, (iii) the detrimental effect of surface roughening is reduced, (iv) geometrical details like grooves, fillets, and holes can be covered more easily [29,40]. Conversely, intense peening treatments can have even adverse effects on the fatigue performance, due to excessive surface roughness and micro-cracks created by fiercely impacting a material whose toughness is limited by the exasperated hardening treatments [38,41]. Moreover, such intense treatments tend to introduce deep in-depth residual stress- and microhardness profiles that are not optimal to prevent surface crack initiation and residual stress relaxation [15,16]. Intense peening treatments are usually applied to Al alloys when fretting rather than plain fatigue is the major concern. In this case, surface roughness increases the real contact area, thus reducing the stresses produced on the surface by the normal and tangential contact loads [42,43].

The present paper is aimed at investigating the influence of the peened surface morphology on the high- and very high-cycle fatigue behaviour of the Al-7075-T651 alloy. For this purpose, pulsating bending fatigue tests ($R = 0.05$) were carried out on smooth samples exploring fatigue lives comprised between 10^5 and 10^8 cycles. Three diverse peening treatments were considered in order to explore different initial residual stress profiles and surface microstructural conditions. An extensive analysis of the residual stress field was carried out by measuring with the X-Ray Diffraction (XRD) technique the residual stress profile before and at the end of the fatigue tests. The surface morphology modifications induced by shot peening were evaluated using an optical profilometer. Particular emphasis was placed on the capability of the shot peening treatments to retard crack initiation or to arrest crack propagation on the surface. Therefore, fatigue crack initiation sites were investigated through Scanning Electron Microscopy (SEM) fractography. The influence of surface roughness on the crack nucleation was quantified by eliminating the surface roughness in some peened specimens through a tribofinishing process.

2. Materials and experimental procedures

The experimentation was performed on the aluminium alloy Al-7075-T651, widely used for aeronautical applications, supplied in the form of 4 mm thick rolled plate. Microstructure and monotonic tensile properties are reported in [29]. The fatigue characterisation was carried out on hourglass specimens whose geometry, according to the standard ISO 3928, is illustrated in Fig. 1. The microstructure has been tested with the stress

axis parallel to the L-direction. The samples present a fillet radius large enough to make any notch fatigue effects negligible.

Part of the specimens was subjected to controlled shot peening: the parameters of the three peening treatments considered are summarized in Table 1. Each treatment was performed using non-metallic beads, which impart to light alloys higher fatigue performance, as compared with steel shots, without introducing undesired galvanic effects [36,]. The basic idea was (i) to apply a commercial peening treatment widely used in the aircraft industry, termed Z150, employing beads of medium-small size (diameter 150 μm), which introduces some surface roughness and a deep cold worked layer (depth $\sim 100 \mu\text{m}$), (ii) to explore an innovative peening treatment, called B120, with smaller ceramic beads leading to a gentle and superficial effect, and (iii) to investigate a fine particle shot peening treatment, termed V40, with very fine glass beads, which is known to greatly enhance the fatigue resistance of aluminium alloys [44].

In order to investigate the effect of the surface roughness induced by shot peening on the fatigue strength, three specimens previously subjected to the treatment B120 and V40 were then subjected to tribofinishing using a controlled vibrating tank with an aqueous medium containing high quality granulates and additives (mainly surfactants). During the process, the specimen surface was periodically observed with an optical microscope to make sure that polishing is stopped just after removing all the dimples created by the shot peening treatments. A material surface layer of approximately $5\div 10 \mu\text{m}$ thickness was removed in this way.

Pulsating ($R = 0.05$) load-controlled 4-point bending fatigue tests were carried out in air, at room temperature, and at a nominal frequency of 110 Hz using a resonant testing machine Rumul Mikrotron 20 kN equipped with a 1 kN load cell. Different stress levels corresponding to fatigue lives in the range between nearly 10^5 and 10^8 cycles were considered. Tests were terminated at 10^8 cycles when no fracture occurred. The fatigue curves corresponding to 50% of failure probability, represented by the S-N curve:



(1)

were determined by fitting the $\log(N_f)$ vs. $\log(\sigma)$ results. The uncertainty range was assumed to be constant and approximated by its centroid value. As a representative value of the scatter, the following expression was used:



(2)

P_{90} , P_{10} denote the 90% and 10% levels of failure probability, respectively.

The modifications of the surface layers produced by the shot peening treatments were investigated through surface roughness and residual stress profile measurements. In this regard, a confocal optical profilometer

Sensofar Plu Neox (plane surface spatial sampling resolution of 0.83 μm , z-axial measurement resolution of 0.02 μm), was used to observe the samples surface. Three dimensional surface topography and roughness were evaluated on an assessment area 636x477 μm^2 . The surface morphology characterization was complemented with contact profilometer scans of the specimen surface over an assessment length of 3 mm, applying a 250 μm cut-off filter to the data.

The residual stress analysis was performed by X-Ray Diffraction (XRD) technique using an AST X-Stress 3000 X-Ray diffractometer. Measurements were made with Cr $K\alpha$ radiation in the longitudinal direction in the gage region. The analysis zone was limited by a collimator of 1 mm^2 in area. The classical $\sin^2\psi$ method was applied for stress evaluation with the use of 9 diffraction angles (2θ) scanned between -45° and $+45^\circ$ for each stress value. The $\langle 311 \rangle$ diffracting planes were chosen (i) in order to obtain high angle measurements (2θ angle 139.0°) with higher strain sensitivity, and (ii) because they do not accumulate significant intergranular stresses and hence exhibit similar behaviour as that of the bulk. Calibration of the system was checked by collecting a diffraction pattern from a standard polycrystalline Al powder prior to conducting the experiment. The in-depth measurements were conducted step-by-step using an electro-polishing device by removing a very thin layer of material in a region (2 mm \times 2 mm) localized at the gauge section of the specimens.

Both initial and stabilized residual stress fields were measured. For this purpose, measurements were performed **after failure** on smooth specimens in a region far enough from the fracture surface (about 2 mm) so that the material rupture was supposed not to have altered the residual stress field [29]. Measurements were carried out on both specimen sides, subjected to tensile and compressive bending stresses, respectively.

3. Experimental results and discussion

3.1 Surface characteristics

The effect on the surface roughness exerted by the shot peening treatments is quantified in Table 2 and 3, where the results of the optical and the contact profilometer measurements, respectively, are summarized. It can be noted that the shot peening treatments increase the surface roughness with the respect to the as-received condition and that the most intense treatment Z150 results in a larger roughness increment with respect to the gentler processes B120 and V40. Considering the gentlest treatments, the B120 variant presents a smaller roughness with respect to V40 despite the employment of larger beads. Conversely, V40 resulted in shallower valleys (lower S_{vk} value), presumably as a result of the lower kinetic energy of the glass shots. The maximum peak to valley height R_t was measured using the contact profilometer because in optical instruments this

parameter is highly affected by spikes and other error sources. Anyway, it is interesting to note that a good estimation of R_t is given by the summation of S_{pk} , S_{vk} and S_k , which are less affected by measurement errors.

The tribofinishing is able to reduce the surface roughness of the peened samples below that of the virgin material. The as-received and the peened variants have a skewness close to zero, index of a symmetric height distribution (i.e. with as many peaks as valleys), while the tribofinished conditions have a negative skewness due to the fact that the surface asperities were removed by the polishing process.

The stress concentration effect exerted by the surface dimples caused by shot peening was estimated according to the following expression proposed by [45]:

(3)

where D_p is the mean spacing between profile peaks (D_p). The value of the estimated K_t is listed in Table 3 for the peened variants.

The surface morphology of the B120, tribofinished B120, V40 and tribofinished V40 conditions is depicted in Fig. 2a-d, respectively. Dimples of smaller size, typical of gentle superficial peening treatments, are visible on the surfaces of the B120 and V40 conditions. Conversely, the superficial structure of impact craters is not visible on the tribofinished variants, thus confirming that the tribofinishing treatment correctly removed the surface roughness induced by the peening treatments.

XRD measurements were carried out on the fatigue samples in order to characterize the residual stress field prior to fatigue testing. The obtained stress profiles are illustrated in Fig. 3a-c for the Z150, B120, and V40 variants, respectively. Three measurements (dotted values) per peening variant were performed in order to account for the variability in the residual stress field. The solid lines represent the average in-depth profile, while the dashed lines identify the $[-\sigma, +\sigma]$ scatter band, where σ is the standard deviation. The repeatability of the residual stress measurements is very good within a depth of about 20 μm , where the fatigue response is mostly dictated [29], while it increases noticeably at higher depths, presumably due to the very elongated grain structure of the sub-superficial material layers that have not undergone recrystallization and hence grain refinement during shot peening. The average residual stress profiles produced by the three shot peening treatments are compared in Fig. 3d.

The peening treatments B120 and V40 display a sub-superficial compressive residual stress peak located nearly 15 μm below the surface and a depth of the surface layer interested by compressive residual stresses equal to about 50 μm . The B120 treatment induces higher residual stresses as compared with the V40 treatment. The

most intense peening treatment Z150 is characterized by lower compressive surface residual stress, by higher sub-superficial compressive peak, and by deeper compressive residual stress profiles (about 90 μm) with respect to the gentler treatments.

3.2 Fatigue curves

The results of the pulsating bending fatigue tests as well as the P_{50} fatigue lines are shown in Fig. 4 in the different material conditions considered and compared with those of the tests carried out on the two tribofinished variants. The parameters representing the fatigue curves corresponding to 50% of failure probability, according to Eq. (1) and the results scatter, expressed by Eq. (2) are listed in Table 4.

All the peening treatments were effective in prolonging the fatigue life of the material as well as in reducing the large scatter in fatigue results displayed by the virgin material. This improvement depends on the applied load, being more remarkable for load levels corresponding to shorter fatigue lives, leading however to higher values of the slope in the P_{50} fatigue line. Therefore, the increment in fatigue resistance due to shot peening steadily declines during fatigue life. The lightest V40 peening treatment, despite lower surface residual stresses and slightly higher roughness, is more effective in improving the plain fatigue resistance with respect to the B120 treatment, which, in turn, performs better than the most intense treatment Z150. Finally, it can be noted that the tribofinished samples displayed a fatigue performance significantly higher with respect to the corresponding peened condition: the increment in fatigue strength due to tribofinishing is about 5% for the V40 and even 20% for the B120 condition. The fact that the tribofinishing improves the fatigue performance of V40 in less extent than B120 condition suggests the hypothesis that the particular surface morphology of the V40 condition, characterized by lower values of the reduced valley depth, exerts a less detrimental effect on the fatigue response as compared with that exhibited by B120. Moreover, the removal of the outer material layer due to tribofinishing seems to have no detrimental effect on the fatigue resistance of the peened samples. Apparently, the microstructural modifications induced by shot peening and investigated in [19-22] do not significantly affect the fatigue behaviour of high-strength Al-alloys. On the other hand, tribofinishing could improve the fatigue performance by eliminating surface micro-cracks generated by the peening treatment.

3.3 Residual stress evolution during fatigue life

Figures 5, 6 and 7 illustrate the evolution of the residual stress field at three loading levels for the Z150 as well as at two loading levels for the B120 and V40 treatment, respectively. Figure 5a (6a, 7a) and 5b (6b, 7b) refer to

the specimen surface subjected to compressive and tensile bending stresses, respectively. It can be noted that some relaxation of the residual stress field occurred on the outer layer (10÷20 µm depth) of the specimen side subjected to compressive bending stresses, the more pronounced the higher the load levels, especially in the B120 and Z150 conditions. Conversely, significantly lower relaxation occurred on the specimen side subjected to tensile bending stresses. This confirms the observations made in [46] that relaxation is more like a “quasi-static” effect, due to the achievement of the material’s plasticization when the compressive bending stresses are superimposed to the compressive surface residuals stress field. Cyclic relaxation seems to be marginal, since the application of tens of millions fatigue cycles do not significantly alter the surface residual stress field on the tensioned side of the samples subjected to the more intense peening treatments. Conversely, the Z150 sample tested at the lowest stress level shows a little tendency to relax also on the tensioned side. The extent of relaxation seems to depend on the number of fatigue cycles rather than on the stress amplitude. This might confirm the observation that residual stress profiles created by intense peening treatment and characterized by a deep subsuperficial residual stress peak are more prone to residual stress relaxation [15,16,46].

Figures 8a and b illustrate the comparison between the initial (prior to tribofinishing) and the stabilized residual stress profiles for the tribofinished B120 and V40 variants, respectively. Due to the limited amount of available tribofinished samples, no (destructive) residual stress measurements were performed just after tribofinishing. In the light of the results of the peened samples, it is however reasonable to assume that the residual stress profiles under tension are close to the initial ones. It can be noted that the material removal exposes on the surface the residual stress that was present at the corresponding depth prior to polishing. Moreover, tribofinishing caused some stress redistribution in the subsuperficial peak, while the depth of the surface layer interested by compressive residual stresses remained nearly unaffected. Residual stress profiles are very similar on the tensioned and the compressed side of the specimen V40, while the compressed side of the B120 samples underwent some residual stress relaxation. Apparently, the residual stress profile of the B120 variant is more prone to relaxation due to plastic flow in compression because the surface layers are subjected to higher compressive residual stresses than those of the V40 variant.

3.4 SEM analysis of fracture surfaces

The fracture surfaces of all the fatigue samples were analyzed with the SEM. The analysis of the unpeened specimens revealed surface crack initiation throughout the entire fatigue life interval explored, even in the very high-cycle fatigue regime, as shown in Fig. 9a. In the peened variants, surface crack initiation was found in the

medium-cycle fatigue regime ($N_f < 1 \times 10^6$), as depicted in Fig. 9b for the B120 condition taken as exemplary of all the peened variants. At longer fatigue lives ($N_f > 2 \times 10^6$), almost all crack initiation sites were found below the surface, at a distance between few microns to 0.2 mm. In this case, the fracture surfaces near the crack initiation sites show a cleavage-like microstructure caused by transcrystalline sliding fracture. This is frequently observed in Al alloys when fatigue tests are conducted under vacuum. In the present work, this evidence can be explained by the fact that the first propagation stages of sub-superficial cracks occur at very low partial pressures of oxygen [31,47,48]. In general, specimens that failed at a number of cycles less than that corresponding to P_{50} probability show, near the subsuperficial initiation site of the main crack, a non-propagating semi-elliptical surface crack nucleated at the root of a dominant peening dimple, as shown in Fig. 10a, b, and c for the Z150, B120 and V40 treatment, respectively. Conversely, specimens that failed at a number of cycles significantly higher than that corresponding to P_{50} probability do not exhibit surface crack initiation, as depicted in Fig. 11a, b, and c for the Z150, B120 and V40 condition, respectively. Apparently, non-propagating cracks, initiated on the surface because of the stress concentration caused by surface roughness, and arrested by the closing effect exerted by compressive residual stresses, might promote crack initiation in the underlying layer, thus leading to a shorter fatigue life.

Figure 11d and e show the fracture surface of the tribofinished B120 and V40 conditions, respectively. It can be noted that in both cases subsuperficial crack initiation occurred and the crack initiation sites are located at a larger depth than those usually observed in the peened variants. Presumably, tribofinishing resulted in a dramatic increment in fatigue strength because surface crack initiation is suppressed by eliminating surface roughness and therefore subsurface crack initiation cannot be promoted by non-propagating surface-cracks. The extension of crystallographic crack growth is larger in the B120 than in the V40 condition. Apparently, the deeper compressive residual stress profile of the B120 condition was more effective in retarding crack propagation towards the surface than that of the V40 variant.

4. Simulation of the behaviour of surface cracks

It has been shown in Section 3 that the surface plays a key role in determining the fatigue response of the peened variants, since, in most cases, cracks initiated on the surface either became the dominant crack leading to the final failure or, after being arrested by the compressive residual stress field, promoted the nucleation of a subsuperficial crack responsible for the eventual fracture. For these reasons, it is desirable to elaborate a method

able to predict the conditions of surface fatigue crack initiation and potential further propagation until final failure.

The first aspect was recently faced by the authors in [49], who conducted multiaxial fatigue tests on both unpeened and peened Al samples. They found that the Crossland criterion, incorporating the surface residual stress field and the stress concentration factor due to surface roughness, is the most suitable method to predict the fatigue behaviour of peened components when the fatigue behaviour is controlled by surface crack initiation. Specifically, the Crossland criterion includes the Von Mises equivalent stress amplitude $\sigma_{VM,a}$, and the maximum hydrostatic pressure p_{max} in a linear equation of the form:

$$\sigma_{VM,a} + \beta_C p_{max} = \alpha_C \sigma_a \quad (4a)$$

where α_C and β_C are material properties that have been determined in [49] at several fatigue lives from fatigue curves performed under tension, torsion and in-phase combined tension-torsion tests. Under bending fatigue tests at stress amplitude σ_a and load ratio R , in the presence of an equibiaxial residual stress field σ^{RS} and surface roughness inducing a stress concentration factor K_t , $\sigma_{VM,a}$ and p_{max} are given by:

$$\sigma_{VM,a} = \sigma_a \sqrt{K_t} \quad (4b)$$

The second issue implies the elaboration of a fracture mechanics approach able to predict near-threshold PSC propagation through the surface layers modified by shot peening. In this regard, Chapetti [50] proposed the following equation to take into account the reduced threshold of PSC due to unsaturated closure:

$$\sigma_a \sqrt{a} = \sigma_{th} \sqrt{a_0} \left(1 - \frac{a_0}{a} \right)^k \quad (5a)$$




where the fatigue crack propagation threshold for PSC σ_{th} is a function of the crack depth a , whereas σ_{th} is the threshold for LC and σ_{th} is the smallest PSC threshold ($a=d$):

$$\sigma_{th} = \sigma_{th} \left(1 - \frac{a_0}{a} \right)^k \quad (5b)$$

where Y is the shape factor (that is equal to 0.75 for the typically observed crack aspect ratio $a/c = 0.75$), σ_{th} is the plain fatigue strength range at high number of cycles to failure, d is the material strongest microstructural barrier. A good estimate of the exponential factor k is given by:


$$k = \frac{\ln \left(\frac{\sigma_{th}}{\sigma_{th}} \right)}{\ln \left(\frac{a}{a_0} \right)} \quad (5c)$$

Values of the material properties to be used in Eqs. (5) and drawn from the literature [51-53] are listed in Table 5.

According to Chapetti's model, the threshold  increases with growing PSC size and asymptotically tends to that of LC when a is much larger than d . Therefore, the condition for PSC propagation is that the applied  is larger than  for any crack depth a .

The calculation of the applied K can be done by using the weight function derived by Wang and Lambert [54] for semi-elliptical surface cracks under non-uniform stresses:


(6a)




where c is the crack surface half-length, t is the plate thickness, m is the weight function and  is the normal stress distribution that is a function of the coordinate x along the crack depth. The stress concentration effect K_t exerted by the surface roughness can be incorporated into K according to the approach proposed by Liu and Mahadevan [55], who suggested considering an effective crack depth a_{eff} expressing an asymptotic dependence on K_t :



(6b)



where D_n is the notch depth, a good estimate thereof is given by the roughness peak to valley height R_t [56]. Since the crack propagates through a non-uniform residual stress field, crack growth occurs under a stress ratio R variable with the crack depth a . As a consequence, it is necessary to modify the applied stress intensity factor in order take into account the mean stress effect on the fatigue crack growth. Noorozi et al. [57] proposed for the near-threshold region the following two-parameter fatigue driving force combining the total stress intensity range, ΔK_{tot} and the total maximum stress intensity factor, $K_{max,tot}$:


(6c)

where K_r is the residual stress intensity factor, $K_{max,appl}$ and $K_{min,appl}$ are the maximum and minimum applied stress intensity factor, respectively.

Figure 12 shows the PSC propagation threshold  (dashed line) as a function of the surface crack depth a . Solid lines refer to the minimum driving force  necessary for MSC nucleated on the surface to overcome the crack-size dependent threshold . The numbers between parentheses indicate the bending stress amplitude

(in MPa) corresponding to the minimum . It can be noted that the two tribofinished variants are the most effective in arresting surface crack propagation, while the Z150 condition suppresses surface PSC growth below a stress amplitude only slightly higher than that of the as-received material. Moreover, the largest non-propagating crack is equal to the strongest microstructural barrier d ($\sim 20 \mu\text{m}$) in all variants, except for the Z150 condition that tolerates non-damaging cracks up to $\sim 60 \mu\text{m}$ depth. This observation is in very good agreement with the fractographic analyses shown in Figs 10.

Figures 13a, b, and c display the experimental fatigue data for the Z150, B120 and V40 conditions, respectively. The location of the crack initiation site (superficial, subsuperficial or subsuperficial assisted by a superficial non-propagating crack) of each fatigue test is also indicated. In addition, solid and dotted lines indicate the conditions for surface crack initiation (expressed by Eq. (4)) and propagation (provided by Eqs. (5) and (6)), respectively. It can be noted that the first condition well represents the mean fatigue curve in the medium-high cycle fatigue regime ($N_f < 2 \times 10^6$), where surface crack initiation is the controlling fatigue phenomenon. At stress amplitudes below the PSC propagation threshold expressed by Eqs. (5-6), surface crack growth is no longer possible. The predicted transition in the location of the nucleation site of the dominant crack is in good agreement with the experimental data shown in Fig. 13. In particular, looking at the Z150 condition, the fact that the driving force  is very close to the threshold  over a large crack depth interval (Fig. 12) can explain the large scatter in the fatigue data around the transition stress amplitude (Fig. 13a): small fluctuations in the characteristics of the surface layers (mainly roughness and residual stresses) result in large differences in the near-threshold PSC propagation.

If the shot peening treatment is able to suppress MSC initiation on the surface and to push it beneath the layer affected by compressive residual stresses, as in the case of the tribofinished specimens and some specimens subjected to B120 and Z150 treatments, Eq. (4) greatly underestimates the fatigue life. If the subsuperficial MSC initiation is promoted by a non-propagating surface crack, the experiments are still in fairly good agreement with Eq. (4) in the high-cycle fatigue regime ($N_f < 5 \times 10^6$), while the fatigue strength in the very high-cycle fatigue regime ($N_f > 10 \times 10^6$) is underestimated. Presumably, in the former case, as soon as a crack initiates on the surface and is arrested, a crack quickly nucleates below the surface leading to the eventual fracture. In the latter case, a longer fatigue life is spent after surface crack arrest to initiate a subsuperficial dominant crack.

5. Conclusions

The plain fatigue strength of shot peened aluminium alloy Al-7075-T651 was experimentally investigated exploring fatigue lives comprised between 10^5 and 10^8 cycles. Experiments were conducted on specimens subjected to three different shot peening treatments. The surface morphology was characterized using an optical profilometer. To quantify the influence of the change in surface morphology induced by shot peening upon the fatigue response, some peened samples were tribofinished with the aim of eliminating surface roughness and preserving the surface residual stress field. XRD measurements were carried out to determine the initial and the stabilized residual stress field. A model has been developed to predict the conditions for surface crack initiation and propagation. The following conclusions can be drawn:

1. Surface layers on the compressed side of the specimens underwent residual stress relaxation due to plastic flow, whose extent depends on the applied bending stress. The samples subjected to the lighter peening treatments show negligible residual stress evolution on the tensioned side. Conversely, the samples subjected to the most intense treatment show some residual stress relaxation on the tensioned side, especially at longer fatigue lives (and thus at lower stress levels).
2. The effect exerted by shot peening is a complicated interaction between residual stresses and surface roughness, greatly impacting the mechanism of fatigue crack initiation and early propagation. In particular, in the very high cycle regime, the initiation of the crack leading to the final failure occurs in the subsurface layers and may be promoted by the presence of non-propagating surface cracks.
3. Shot peening conducted at low intensities with small beads is more effective in incrementing the fatigue resistance as compared to more intense treatments with larger shots, since it causes a lower surface roughening and induces the maximum compressive residual stress as close as possible to the surface. In this way, higher resistance to MSC initiation and PSC propagation as well as to residual stress relaxation is imparted to the surface layers.
4. The most effective surface treatment is a combination of a gentle and superficial shot peening with a tribofinishing process. The extent of the additional improvement due to roughness elimination depends on the type of shot peening, being more significant if the layer interested by compressive residual stresses is deeper.

References

- [1] Ludtka GM, Laughlin DE. The effect of solute content on the slip behavior in 7xxx series aluminum alloys. *Metallurgical Transactions* 1981;12A:2083-2091.
- [2] Lütjering G. Influence of processing on microstructure and mechanical properties of (α + β) titanium alloys. *Mater. Sci. Engng.* 1998;A243:32-45.
- [3] Suresh S, Ritchie RO. The propagation of short fatigue cracks. *Int Metals Rev* 1984;29(6):445–76.
- [4] Lütjering G. Property optimization through microstructural control in titanium and aluminum alloys. *Mater. Sci. Engng.* 1999;A263:117-126.
- [5] Mughrabi H. Cyclic slip irreversibilities and the evolution of fatigue damage. *Metallurgical and materials transactions* 2009;40A:1257-1279.
- [6] Gao Y, Lu F, Yao M. Influence of mechanical surface treatments on fatigue property of 30CrMnSiNi2A steel. *Surface Engineering* 2005;21:325-328.
- [7] Susmel L, Tovo R, Lazzarin P. The mean stress effect on the high-cycle fatigue strength from a multiaxial fatigue point of view. *Int. J. Fatigue* 2005;27:928-943.
- [8] Ritchie RO. Mechanisms of fatigue-crack propagation in ductile and brittle solids. *Int. J. Fracture* 1999;100:55-83.
- [9] Benedetti M, Heidemann J, Peters JO, Lütjering G. Influence of sharp microstructural gradients on the fatigue crack growth resistance of $\alpha + \beta$ and near- α titanium alloys. *Fatigue Fract Engng Mater Struct* 2005;28:909-922.
- [10] de los Rios ER, Walley A, Milan MT, Hammersley G. Fatigue crack initiation and propagation on shot-peened surfaces in A316 stainless steel. *Int. J. Fatigue* 1995;17:493-499.
- [11] Rodopoulos CA, Curtis SA, de los Rios ER, SolisRomero J. Optimisation of the fatigue resistance of 2024-T351 aluminium alloys by controlled shot peening—methodology, results and analysis. *Int. J. Fatigue* 2004;26:849-856.
- [12] Hammond DW, Meguid SA. Crack propagation in the presence of shot-peening residual stresses. *Eng Fract Mech* 1990;37:373–387.
- [13] Cerny I, Sis J, Mikulova D. Short fatigue crack growth in an aircraft Al-alloy of a 7075 type after shot peening. *Surface&Coatings Technology* 2014;243:20-27.
- [14] Riemelmoser FO, Pippan R. Consideration of the mechanical behaviour of small fatigue cracks. *Int J Fract* 2002;118(3):251–70.

- [15] McClung RC. A literature survey on the stability and significance of residual stresses during fatigue. *Fatigue Fract Eng Mater Struct* 2007;30:173–205.
- [16] Asquith DT, Hattingh DG, James MN, Yates JR. Re-orientation of residual strains under cyclic loading. *Fatigue* 2007, Queens' College, Cambridge, 2007.
- [17] Wagner L. Mechanical surface treatments on titanium, aluminum and magnesium alloy. *Mater Sci Eng* 1999;A263:210–216.
- [18] Wagner L, Lütjering G. Influence of shot peening on the fatigue behaviour of Ti-alloys. In: *Shot peening*. Oxford: Pergamon Press; 1981. p. 453–60.
- [19] E. R. de los Rios, M. Trooll and A. Levers (1999) Improving the fatigue crack resistance of 2024-T351 aluminium alloy by shot peening. In: *Proceedings Ceas Forum: Life Extension— Aerospace Technology Opportunities*, Churchill College, Cambridge, pp. 26.1–26.8.
- [20] Honda T, Ramulu M, Kobayashi AS. Effect of Shot Peening on Fatigue Crack growth in 7075-T7351. *The Journal of ASTM International* 2005;2:1-14.
- [21] Zupanc U, Grum J. Surface integrity of shot peened aluminium alloy 7075-T651. *Strojiniski Vestnik – J Mech Eng* 2011;57:379–84.
- [22] Garipey A, Bridier F, Hoseini M, Bocher P, Perron C, Levesque M. Experimental and numerical investigation of material heterogeneity in shot peened aluminium alloy AA2024-T351. *Surface&Coatings Technology* 2013;219:15-30.
- [23] Benedetti M, Fontanari V, Höhn B, Oster P, Tobie T. Influence of shot peening on bending tooth fatigue limit of case hardened gears. *Int J Fatigue* 2002;24:1127–36.
- [24] Mikova K, Bagherifard S, Bokuvka O, Guagliano M, Trsko L. Fatigue behavior of X70 microalloyed steel after severe shot peening. *Int. J. Fatigue* 2013;55:33-42.
- [25] Wang S, Li Y, Yao M, Wang R. Fatigue limits of shot-peened metals. *J Mater Process Technol* 1998;73:57–63.
- [26] Ochi Y, Masaki K, Matsumura T, Sekino T. Effect of shot-peening treatment on high cycle fatigue property of ductile cast iron. *Int J Fatigue* 2001;23:441–448.
- [27] Torres MAS, Voorwald HJC. An evaluation of shot peening, residual stress and stress relaxation on the fatigue life of AISI 4340 steel. *Int. J. Fatigue* 2002;24:877-886.
- [28] Shiozawa K, Lu L. Very high-cycle fatigue behaviour of shot-peened high-carbon-chromium bearing steel. *Fatigue Fract Eng Mater Struct* 2002;25:813–822.

- [29] Benedetti M, Fontanari V, Scardi P, Ricardo CLA, Bandini M. Reverse bending fatigue of shot peened 7075-T651 aluminium alloy: the role of residual stress relaxation. *Int J Fatigue* 2009;31:1225–1236.
- [30] Pyttel B, Brunner I, Kaiser B, Berger C, Mahendran M. Fatigue behaviour of helical compression springs at a very high number of cycles – Investigation of various influences. *Int. J. Fatigue* 2014;60:101-109.
- [31] Wang QY, Kawagoishi N, Chen Q. Fatigue and fracture behaviour of structural Al-alloys up to very long life regimes. *Int J Fatigue* 2006;28:1572–1576.
- [32] Zhao T, Jiang Y. Fatigue of 7075-T651 aluminum alloy. *Int J Fatigue* 2008;30:834–49.
- [33] Bian JC, Tokaji K, Ogawa T. Notch sensitivity of aluminium–lithium alloys in fatigue. *J Soc Mater Sci Jpn* 1994;43(490):840–6 [in Japanese].
- [34] Miller KJ. The two thresholds of fatigue behaviour. *Fatigue Fract Eng Mater Struct* 1993;16(9):931–9.
- [35] Was GS, Pelloux RM. The effect of shot peening on the fatigue behavior of alloy 7075-T6. *Metall Mater Trans A* 1979;10(5):656–8.
- [36] Mutoh Y, Fair GH, Noble B, Waterhouse RB. The effect of residual stresses induced by shot peening on fatigue crack propagation in two high strength aluminium alloys. *Fatigue Fract Eng Mater Struct* 1987;10(4):261–72.
- [37] Sharp PK, Clayton JQ, Clark G. The fatigue resistance of peened 7050-T7451 aluminium alloy-repair and retreatment of a component surface. *Fatigue Fract Eng Mater Struct* 1994;17(3):243–52.
- [38] Benedetti M, Bortolamedi T, Fontanari V, Frenzo F. Bending fatigue behaviour of differently shot peened Al 6082 T5 alloy. *Int J Fatigue* 2004;26:889–97.
- [39] Gao YK. Improvement of fatigue property in 7050–T7451 aluminium alloy by laser peening and shot peening. *Mater Sci Eng* 2011;A528:3823–3828.
- [40] Benedetti M, Fontanari V, Santus C, Bandini M. Notch fatigue behaviour of shot peened high-strength aluminium alloys: experiments and predictions using a critical distance method. *Int J Fatigue* 2010;32:1600–1611.
- [41] Luo W, Noble B, Waterhouse RB. The effect of shot peening intensity on the fatigue and fretting behaviour of an aluminium alloy. In: Niku-Lari A, editor. *Advances in surface treatments*, vol. 2. Oxford: Pergamon Press; 1988. p. 145–53.
- [42] Waterhouse RB, Trowsdale AJ. Residual stress and surface roughness in fretting fatigue. *J Phys D* 1992;25:A236–7.

- [43] Vazquez J, Navarro C, Dominguez J. Experimental results in fretting fatigue with shot and laser peened Al 7075-T651 specimens. *Int J Fatigue* 2012;40:143–153.
- [44] Oguri K. Fatigue life enhancement of aluminum alloy for aircraft by Fine Particle Shot Peening (FPSP). *J. Mat. Proc. Technol.* 2011;211:1395-1399.
- [45] Li JK, Yao Mei, Wang Duo, Wang Renzhi. An analysis of stress concentration caused by shot peening and its application in predicting fatigue strength. *Fatigue Fract Eng Mater Struct* 1992;15(12):1271–1279.
- [46] Benedetti M, Fontanari V, Monelli BD. Numerical simulation of residual stress relaxation in shot peened high-strength aluminium alloys under reverse bending fatigue. *ASME J. Engng Mater. Techn.* 2010;132:011012.
- [47] Pyttel B, Schwerdt D, Berger C. Very high cycle fatigue – Is there a fatigue limit?. *Int J Fatigue* 2012;33:49–58.
- [48] Bonakdar A, Wang F, Williams JJ, Chawla N. Environmental effects on fatigue crack growth in 7075 Aluminum alloy. *Metallurgical and Material Transactions* 2012;43A:2799-2809.
- [49] Benedetti M, Fontanari V, Bandini M, Taylor D. Multiaxial fatigue resistance of shot peened high-strength aluminum alloys. *Int J Fatigue.* 2014;61:271-282.
- [50] Chapetti MD. Fatigue propagation threshold of short cracks under constant amplitude loading. *Int J Fatigue* 2003;25:1319–1326.
- [51] Lankford J. The growth of small fatigue cracks in 7075-T6 aluminum. *Fatigue Fract Eng Mater Struct* 1982;5:233–248.
- [52] Noroozi AH, Glinka G, Lambert S. Prediction of fatigue crack growth under constant amplitude loading and a single overload based on elasto-plastic crack tip stresses and strains. *Engng. Fract. Mech.* 2008;75:188-206.
- [53] Benedetti M, Fontanari V, Monelli BD. Plain fatigue resistance of shot peened high strength aluminium alloys: effect of loading ratio. *Procedia Engineering* 2010;2(1):397-406.
- [54] Wang X, Lambert S. Stress intensity factors for low aspect ratio semi-elliptical surface cracks in finite-thickness plates subjected to nonuniform stresses. *Engng. Fract. Mech.* 1995;51:517-532.
- [55] Liu Y, Mahadevan S. Fatigue limit prediction of notched components using short crack growth theory and an asymptotic interpolation method. *Engng. Fract. Mech.* 2009;76:2317-2331.

- [56] Xiang Y, Liu Y. Mechanism modelling of shot peening effect on fatigue life prediction. *Fatigue Fract Eng Mater Struct* 2009;33:116-125.
- [57] Noroozi AH, Glinka G, Lambert S. A two parameter driving force for fatigue crack growth analysis. *Int J Fatigue* 2005;27:1277–1296.

Tables

Table 1: Shot peening parameters.

Treatment	Material	Bead size [μm]	Bead hardness [HV ₁]	Bead composition	Almen intensity	Angle of impingment	Coverage [%]
Z150	Ceramic	150÷210	700	ZrO ₂ 67%	12 N	90°	100
B120	Ceramic	63÷125		SiO ₂ 31%	4.5 N		
V40	Glass	40÷70	550	SiO ₂ 31% Na ₂ O 14%	4.2 N		

Table 2: 3D surface roughness properties.

Condition	S _a [μm]	S _q [μm]	S _{sk}	S _{ku}	S _{pk} [μm]	S _k [μm]	S _{vk} [μm]
As-received	0.29	0.38	0.19	5.98	0.59	0.81	0.41
Z150	3.79	4.83	0.29	8.60	8.09	11.56	3.56
B120	1.24	1.54	0.14	3.03	1.75	3.96	1.42
B120 trib.	0.19	0.26	-1.21	12.17	0.29	0.55	0.38
V40	1.33	1.66	-0.01	2.96	2.12	4.23	1.24
V40 trib.	0.17	0.23	-1.30	12.52	0.28	0.49	0.33

S_a: average roughness; S_q: root mean square roughness; S_{sk}: skewness; S_{ku}: kurtosis; S_{pk}: reduced peak height; S_k: core roughness depth; S_{vk}: reduced valley depth

Table 3: 2D surface roughness properties.

Condition	R _t [μm]	D _p [μm]	K _t
Z150	21.29	200	1.22
B120	7.12	110	1.11
V40	7.66	100	1.14

R_t: maximum peak to valley height; D_p: mean spacing of adjacent local peaks; K_t: stress concentration factor due to surface roughness

Table 4: Principal results of fatigue tests.

Condition	<i>s</i>	σ_{0P50} [MPa]	$\square\sigma$
As-received	33	200	1:1.22
Z150	20	315	1:1.17
B120	12	555	1:1.19
V40	12	590	1:1.10

s, σ_{0P50} : slope and y-intercept of the Wöhler curve according to Eq. (1), $\square\sigma$: results scatter according to Eq. (2)

Table 5: Material properties used in Eqs. (5).

Property	Value	Ref.
d	0.018 mm	[51]
$\Delta K_{thR} (R = 0)$	2.4	[52]
$(R = 0)$	254 MPa	[53]

Figure captions

Figure 1. Geometry of the smooth hourglass specimen used in this study for bending fatigue tests. All dimensions are given in mm.

Figure 2. Surface topographies acquired through optical profilometer. (a) B120 peened, (b) B120 peened and tribofinished, (c) V40 peened, (d) V40 peened and tribofinished. The assessment area is $636 \times 477 \mu\text{m}^2$.

Figure 3. Initial longitudinal residual stress profiles of the peened variants measured by XRD technique. Three measurements per peened variant were carried out in order to account for the variability in the residual stress field. (a) Z150, (b) B120, (c) V40 conditions. Beside experimental data, the mean in-depth profile and the $[-\sigma, \sigma]$ scatter band are shown. (d) Comparison among the mean initial residual stress profiles created by the three peening treatments.

Figure 4. Pulsating bending fatigue curves of the as-received and peened conditions. Run-out tests are marked by arrows.

Figure 5. Evolution of the longitudinal residual stress profile during fatigue life in samples subjected to Z150 treatment. (a) Tensioned, (b) compressed side. Specimen tested at 280 (320, 400) maximum stress MPa failed after 50.6×10^6 (5.1×10^6 , 106000) cycles. Dashed lines refer to mean and $[-\sigma, \sigma]$ scatter band of the initial residual stress profile.

Figure 6. Evolution of the longitudinal residual stress profile during fatigue life in samples subjected to B120 treatment. (a) Tensioned, (b) compressed side. Specimen tested at 270 (400) maximum stress MPa failed after 44.6×10^6 (530000) cycles. Dashed lines refer to mean and $[-\sigma, \sigma]$ scatter band of the initial residual stress profile.

Figure 7. Evolution of the longitudinal residual stress profile during fatigue life in samples subjected to V40 treatment. (a) Tensioned, (b) compressed side. Specimen tested at 290 (420) MPa maximum stress failed after 22.8×10^6 (390000) cycles. Dashed lines refer to mean and $[-\sigma, \sigma]$ scatter band of the initial residual stress profile.

Figure 8. Evolution of the longitudinal residual stress profile during fatigue life in peened and tribofinished samples. (a) B120, (b) V40 peening. Specimens were tested at 360 MPa maximum stress and failed after (a) 13.3×10^6 and 3.3×10^6 cycles. Dashed lines refer to mean and $[-\sigma, \sigma]$ scatter band of the initial residual stress profile.

Figure 9. Fracture surface with surface fatigue crack initiation site. (a) as-received ($\sigma_a = 133$ MPa, $N_f = 25.0 \times 10^6$), (b) B120 ($\sigma_a = 209$ MPa, $N_f = 139000$)

Figure 10. Fracture surface with subsurface initiation site of the dominant fatigue crack and neighbouring non-propagating surface crack (the crack front is marked by small arrows). (a) Z150 ($\sigma_a = 133$ MPa, $N_f = 48.2 \times 10^6$), (b) B120 ($\sigma_a = 133$ MPa, $N_f = 9.0 \times 10^6$), (c) V40 ($\sigma_a = 152$ MPa, $N_f = 3.6 \times 10^6$).

Figure 11. Fracture surface with subsurface crack initiation site. (a) Z150 ($\sigma_a = 171$ MPa, $N_f = 2.7 \times 10^6$), (b) B120 ($\sigma_a = 162$ MPa, $N_f = 6.3 \times 10^6$), (c) V40 ($\sigma_a = 162$ MPa, $N_f = 2.7 \times 10^6$), (d) B120 tribofinished ($\sigma_a = 171$ MPa, $N_f = 13.3 \times 10^6$), (e) V40 tribofinished ($\sigma_a = 171$ MPa, $N_f = 3.3 \times 10^6$).

Figure 12. Comparison between the crack-size dependent threshold for PSC propagation ΔK_{th} and the minimum driving force $\Delta \kappa$ necessary for surface crack growth. The number between parenthesis are the bending stress amplitude at which $\Delta \kappa$ is calculated.

Figure 13. Experimental fatigue data sorted by the location of the crack initiation site. (a) Z150, (b) B120, and (c) V40 peening treatment. Closed symbols: superficial crack initiation; open symbols: subsuperficial crack initiation (open symbols); half-closed symbols: subsuperficial crack initiation promoted by a non-propagating surface crack. The condition for surface crack initiation is represented by the solid lines (expressed by Eq. (4)),

while the dotted lines indicate the threshold stress amplitude (identified by Eqs. (5) and (6)) below which surface cracks are arrested.